Epitaxial Electrodeposition of Pb−Tl−O Superlattices on Single-Crystal Au(100)

Hiten M. Kothari, Alexey A. Vertegel, Eric W. Bohannan, and Jay A. Switzer*

Department of Chemistry and Graduate Center for Materials Research, University of Missouri−Rolla, Rolla, Missouri 65409-1170

Received January 15, 2002. Revised Manuscript Received April 23, 2002

Superlattices in the Pb−Tl−O system with modulation wavelengths varying from 5.2 to 18.9 nm were epitaxially electrodeposited on single-crystal Au(100) by periodically pulsing the current anodically between 0.05 and 5 mA/cm^2. The films were grown at room temperature from an aqueous solution of 0.005 M $TlNO_3$ and 0.1 M $Pb(NO_3)_2$ in 5 M NaOH. Bulk films deposited at current densities of 0.05 and 5 mA/cm^2 have compositions of approximately $Pb_{0.46}Tl_{0.54}O_{1.7}$ and $Pb_{0.74}Tl_{0.26}O_{1.9}$, respectively. X-ray diffraction (XRD) results show a strong [100] out-of-plane orientation for the electrodeposited films. Seven orders of satellite peaks are seen in the XRD pattern for a superlattice with a modulation wavelength of 18.9 nm. Azimuthal scans for the (111) reflection of Au and Pb−Tl−O show that the film is rotated 45° in-plane with respect to the substrate. The in-plane rotation of 45° reduces the lattice mismatch between the Au substrate and the deposited superlattice from 31% to −7.6%. An epitaxial relationship consistent with this rotation is Pb−Tl−O(100)[011]// Au(100)[010].

Introduction

Superlattices are a type of crystalline material abruptly modulated with respect to composition or structure or both. Multilayers and superlattices are both modulated materials but superlattices have the additional constraint of being crystallographically coherent.[1] Superlattice structures of semiconductors,[2,3] ceramics,[4] and metals[5] have traditionally been deposited using techniques such as molecular beam epitaxy, metal−organic chemical vapor deposition, physical vapor deposition, and reactive magnetron sputtering.

Metallic and ceramic superlattices can result in enhanced mechanical properties compared to the bulk element or alloy. Significant enhancement in hardness makes these structures ideal for protective surface coatings.[6,7] Giant magnetoresistance[8,9] (GMR) in magnetic multilayers has opened a new field for electronics called spintronics based on the spin of the electron.[10] Giant magnetoresistance and magnetic tunnel junction (MTJ) structures are being considered for applications as magnetic field sensors, read heads, and nonvolatile memory.[9] Semiconductor superlattices fabricated by sandwiching a lower band gap material between layers of a larger band gap material cause fundamental changes in the optical and electronic properties of the material.[11,12] These structures are used for quantum lasers, optical switches, high-speed optical modulators, avalanche photodetectors, and fast transistors.[13,14]

Most of the work on electrodeposited superlattices has concentrated on growing metallic superlattices with enhanced elastic and plastic properties, improved wear resistance, and magnetic anisotropy.[15,16] In addition to its cost-effectiveness, electrochemistry offers a unique advantage over other techniques by minimizing interdiffusion across interfaces because of the low processing temperatures. It also offers better control over the film thickness, which can be precisely controlled from the amount of charge passed. Recently, there have been reports of electrochemically deposited semiconductor superlattices made by electrochemical atomic layer epitaxy.[17]

Our group has previously concentrated on growing electrodeposited ceramic superlattices by periodically pulsing the current or potential during deposition.

* To whom correspondence should be addressed. E-mail: jswitzer@umr.edu.

(1) Schuller, I. K. *Phys. Rev. Lett.* **1980**, *44*, 1597.
(2) Chang, L. L. *J. Vac. Sci. Technol. B* **1983**, *1*, 120.
(3) Leavens, C. R.; Taylor, R. *Interfaces, Quantum Wells, and Superlattices*; Plenum: New York, 1988; Vol. 179.
(4) Imai, F.; Kunimori, K.; Nozoye, H. *Appl. Phys. Lett.* **1993**, *63*, 2638.
(5) Fujii, Y. *Metallic Superlattices: Artificially Structured Materials*; Shinjo, T., Takada, T., Eds.; Elsevier: Amsterdam, 1987.
(6) Tench, D. M.; White, J. T. *J. Electrochem. Soc.* **1990**, *137*, 3061.
(7) Mirkarimi, P. B.; Hultman, L.; Barnett, S. A. *Appl. Phys. Lett.* **1990**, *57*, 2654.
(8) Baibich, B. B.; Broto, J. M.; Fert, A.; Nguyen Van Dau, F.; Petroff, P.; Etienne, P.; Cruezet, G.; Friedrich, A.; Chazeles, J. *Phys. Rev. Lett.* **1988**, *61*, 2472.
(9) Prinz, G. A. *Science* **1998**, *282*, 1660.
(10) Wolf, S. A; Awschalom, D. D.; Buhrman, R. A.; Daughton, J. M.; Von Molnar, S.; Roukes, M. L.; Chtchelkanova, A. Y.; Treger, D. M. *Science* **2001**, *294*, 1488.
(11) Davies, J. H. *The Physics of Low-Dimensional Semiconductors: An Introduction*; Cambridge University Press: Cambridge, 1988.
(12) Kelley, M. J. *Low-Dimensional Semiconductors: Materials, Physics, Technology, Devices*; Oxford University Press: Oxford, 1995.
(13) Chemla, D. S. *Phys. Today* **1985**, *38*, 58.
(14) Ploog, K. *Phys. Technol.* **1998**, *19*, 196.
(15) Moffat, T. P. *J. Electrochem. Soc.* **1995**, *142*, 3767.
(16) Schwarzacher, W.; Lashmore, D. S. *IEEE Trans. Magn.* **1996**, *32*, 3133.
(17) Stickney, J. L. Electrochemical Atomic Layer Epitaxy. In *Electroanalytical Chemistry, A Series of Advances*; Marcel Dekker: New York, 1999.

10.1021/cm020042h CCC: $22.00
Published on Web 05/24/2002

Because the superlattices were deposited on polycrystalline substrates, they had columnar microstructures with no in-plane order. We have previously reported growing superlattices of Pb−Tl−O[18,19] and defect-chemistry superlattices based on Tl_2O_3[20] on polycrystalline substrates. We have also analyzed the current−time transients during the deposition to estimate the composition profile of the electrodeposited layers.[21] In this work we report the epitaxial electrodeposition of superlattices in the Pb−Tl−O system on single-crystal Au(100) by periodically pulsing the current density during deposition. The in-plane and out-of-plane orientation of the Pb−Tl−O superlattice is controlled by the Au(100) substrate.

Experimental Section

Electrochemical experiments were carried out using an EG&G Princeton Applied Research (PAR) model 273A potentiostat/galvanostat in conjunction with the EG&G M270 software. The cell configuration consisted of a platinum counter electrode and a standard calomel reference electrode (SCE) placed as close as possible to the working electrode. The deposition solution contained 0.005 M $TlNO_3$ and 0.1 M $Pb(NO_3)_2$ in 5 M NaOH prepared using deionized water **(caution: thallium and lead compounds are extremely toxic)**. The solution was allowed to equilibrate for 24 h. The films were grown by pulsing the current anodically between 0.05 and 5 mA/cm^2 from a well-stirred solution to a thickness of 100 bilayers. The dwell times at the respective current densities were varied depending on the thickness desired. The thickness was calculated using Faraday's equation.

The working electrode consisted of an Au(100) single crystal purchased from Monocrystal Company having a diameter of 10 mm and a thickness of 2 mm. A gold wire fitted around the single crystal served as an electrical contact to the working electrode. The working electrode was placed in solution using the meniscus method. The Au(100) single crystal was electropolished and annealed in a hydrogen flame prior to deposition. Electropolishing was carried out in a moderately stirred solution of 50 vol % ethanol, 25 vol % ethylene glycol, and 25 vol % concentrated HCl at 55 °C. A constant anodic current of 0.75 A/cm^2 was applied for 30−60 s. A graphite electrode served as the counter electrode. Pb−Tl−O films were removed by etching in 1 M ascorbic acid and the Au crystal reused after flame annealing.

X-ray diffraction experiments were carried out with a Philips X'Pert Materials Research Diffractometer (MRD) system. The Cu tube source was operated at 45 kV and 40 mA. Three types of experiments were performed. Phase analysis using 2θ scans to evaluate the film texture and modulation wavelength were carried out using a two-bounce Ge(220) asymmetric hybrid monochromator 2X (PW3147/00, Philips) on the incident beam side (primary optic) and 0.18° parallel plate collimator (PW3098/18, Philips) as the secondary optic on the detector side. The hybrid monochromator consists of a Göbel X-ray mirror and a two-crystal channel cut Ge(220) two-bounce monochromator. The parabolic-shaped graded multilayer X-ray mirror collimates the divergent beam from a line focus of the X-ray tube to a quasi-parallel beam. The hybrid monochromator gives pure Cu $K\alpha_1$ radiation with a divergence of 25 arcseconds. The scans were acquired with a 2θ step size of 0.01° and a dwell time of 1 s/step. To obtain improved statistics around the satellite positions for the superlattice, the scans were acquired around the Bragg peaks with 2θ step size of 0.01° and a dwell time of 25 s/step. Rocking curves were obtained with the 2 × Ge(220) hybrid monochromator as the primary optic and a rocking curve attachment (PW3120/60, Philips) as the secondary optic. A step size of 0.01° for the ω axis with a dwell time of 1 s/step was used. X-ray pole figures and azimuthal scans were obtained using an adjustable crossed slit collimator (PW3094/62, Philips), 2 × 2 mm, as the primary optic and a 0.27° parallel plate collimator (PW3098/27) with a graphite monochromator (PW3121/00) as the secondary optic.

X-ray photoelectron spectroscopy (XPS) experiments were performed on an AXIS 165, Kratos Analytical high-resolution spectrometer. The measurements were carried out in ultrahigh vacuum conditions (10^{-9} Torr) using non-monochromatic Mg Kα (250 W) radiation. The samples were sputter-cleaned using Ar ions at an approximate rate of 15 Å/min for 2 min using a Kratos Minibeam ion sputtering gun operated at a beam current of 15 mA and a beam voltage of 3 kV. The values of the binding energies (BE) were referenced to that of the C 1s peak at 284.6 eV. The error for the observed values of the binding energies is estimated to be about ±0.5 eV. The scans were acquired with a step of 0.1 eV and a dwell time of 0.5 s.

Results and Discussion

Varying the current or potential controls the composition of electrodeposited Pb−Tl−O. The standard reduction potentials for Tl_2O_3 and PbO_2 are −0.22 and 0.04 V, respectively, versus SCE. This implies that a 1 M NaOH solution containing Tl^+ should produce Tl_2O_3 at potentials positive of −0.22 V vs SCE, and a 1 M NaOH solution containing Pb^{2+} should produce PbO_2 at potentials positive of 0.04 V vs SCE. A solution with both Tl^+ and Pb^{2+} gives Pb−Tl−O with varying Pb/Tl ratios depending on the applied potential and the concentration of the ions in the solution. Pb−Tl−O superlattices are deposited by adjusting the concentration of Tl^+ so that the deposition of Tl_2O_3 is mass-transport-limited at the potential where PbO_2 deposition occurs.[22,23] The above analysis suggests that the Tl content in the films deposited at a potential before the mass-transfer-limited potential for Tl_2O_3 should be higher compared to that of films deposited at a more positive potential. The Pb content increases as the applied potential becomes more positive.

The Pb−Tl−O materials in this work have the fluorite structure with space group $Fm3m$. Figure 1A,B shows the X-ray scans for 2-μm-thick films grown at an applied anodic current density of 0.05 and 5 mA/cm^2, respectively, on the Au(100) substrate. The lattice parameters for the films grown at 0.05 and 5 mA/cm^2 are 0.53320 and 0.53383 nm, respectively. Hence, the lattice mismatch between the films grown under these conditions is 0.12%. The scans show a strong [100] out-of-plane orientation for both films. Azimuthal scans showed a strong in-plane orientation with only the peaks corresponding to the [100] orientation visible.

The steady-state potential for the two films stabilized at approximately 55 and 270 mV vs SCE, respectively. The values of steady-state potential are consistent with those reported elsewhere at the respective current densities.[18,19,22] The lattice parameters and the compositions measured by energy-dispersive spectroscopy (EDS)

(18) Switzer, J. A.; Shane, M. J.; Phillips, R. P. *Science* **1990**, *247*, 444.
(19) Switzer, J. A.; Raffaelle, R. P.; Phillips, R. J.; Hung, C.-J.; Golden T. D. *Science* **1992**, *258*, 1918.
(20) Switzer, J. A.; Hung, C.-J.; Breyfogle, B. E.; Shumsky, M. G.; Van Leeuwen, R.; Golden T. D. *Science* **1994**, *264*, 1505.
(21) Switzer, J. A.; Phillips, R. J.; Golden T. D. *Appl. Phys. Lett.* **1995**, *66*, 819.
(22) Phillips, R. J.; Golden T. D.; Shumsky, M. G.; Bohannan, E. W.; Switzer, J. A. *Chem. Mater.* **1997**, *9*, 1670.
(23) Switzer, J. A. *The Electrochemistry of Nanostructures: Preparation and Properties*; Hodes, G., Ed.; Wiley-VCH: Weinheim, 2001.

Table 1. Lattice Parameters and Film Compositions Measured by Energy-Dispersive Spectroscopy (EDS) and Anodic Stripping Voltammetry (ASV) on a Metals-Only Basis for Pb−Tl−O Films as a Function of the Deposition Current Density

applied current density (mA/cm^2)	lattice parameter (nm)	theoretical[a] density (g/cm^3)	EDS[b]			ASV[c]		
			Pb at. %	Tl at. %	film composition	Pb at. %	Tl at. %	film composition
0.05	0.53320	10.20	46	54	$Pb_{0.46}Tl_{0.54}O_{1.7}$	54	46	$Pb_{0.54}Tl_{0.46}O_{1.8}$
5	0.53383	10.34	74	26	$Pb_{0.74}Tl_{0.26}O_{1.9}$	79	21	$Pb_{0.79}Tl_{0.21}O_{1.9}$

[a] Based on the atomic percentages from EDS. [b] EDS data from ref 19. [c] ASV data from ref 22. The O compositions were calculated by assuming an oxidation state of +4 for Pb and +3 for Tl.

Table 2. XPS Binding Energies and Compositions Determined on a Metals-Only Basis for Pb−Tl−O Films as a Function of the Deposition Current Density

applied current density (mA/cm^2)	Pb $4f_{7/2}$					Tl $4f_{7/2}$					film[b] composition
	BE[a] (eV)	fwhm (eV)	peak area (CPS)	RSF	at. %	BE (eV)	fwhm (eV)	peak area (CPS)	RSF	at. %	
0.05	137.2	1.25	61136	5.19	45	117.6	1.30	69235	4.80	55	$Pb_{0.45}Tl_{0.55}O_{1.7}$
5	137.1	1.25	115690		80	117.5	1.25	26677		20	$Pb_{0.80}Tl_{0.20}O_{1.9}$

[a] The values of the binding energies (BE) were referenced to that of the C 1s peak at 284.6 eV.[25,26] The error for the observed values of the binding energies is estimated to be about ±0.5 eV. [b] The film composition was based on the percentage of atomic composition of Pb and Tl, which are obtained from the quantitative analysis of the peak areas using the reduced sensitivity factors (RSF) shown for each element. The O compositions were calculated by assuming an oxidation state of +4 for Pb and +3 for Tl.

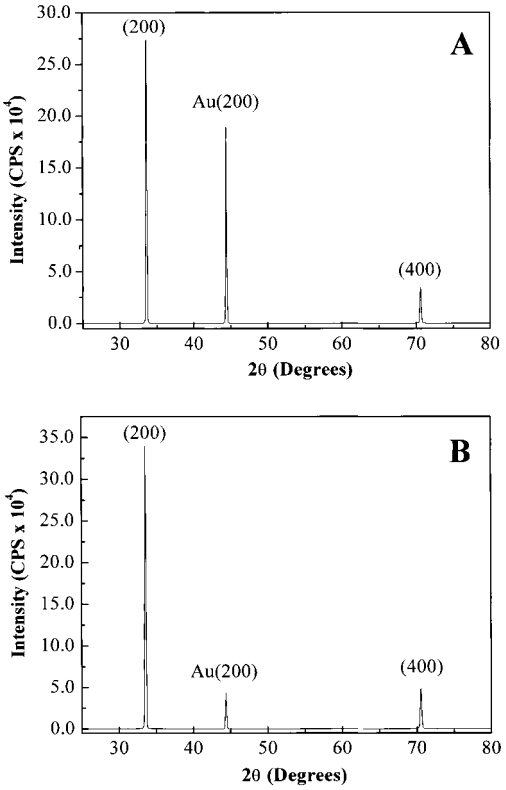

Figure 1. X-ray 2θ scans for 2-μm-thick films of Pb−Tl−O on Au(100) at an applied anodic current density of (A) 0.05 and (B) 5 mA/cm^2. The scans were acquired using pure Cu $K\alpha_1$ radiation as the X-ray source. A strong [100] out-of-plane orientation is evident in the patterns. The lattice parameter for the film at 0.05 mA/cm^2 is 0.53320 nm while that at 5 mA/cm^2 is 0.53383 nm.

and anodic stripping voltammetry (ASV) for the films grown under galvanostatic conditions are shown in Table 1. The compositions of films deposited at different current densities determined by using EDS have been reported by Switzer et al.[19] The L-lines for thallium (10.27 keV) and lead (10.55 keV) were used to calculate the metals-only composition from the EDS measurements. The Pb and Tl compositions, also on a metals-only basis, were later verified by Phillips et al.[22] using ASV. In both cases, the O content was calculated by assuming oxidation states of +4 and +3 for Pb and Tl, respectively. An increase in the Pb content of the deposited films is evident as the applied potential becomes more positive. These results confirm that changing the applied current density changes the film composition.

X-ray photoelectron spectroscopy (XPS) was used to probe the oxidation state of the metal ions in the films and to determine the Pb and Tl contents. Table 2 lists the binding energies for the observed peak positions in the XPS spectrum for various elements in the system. The energy spectrum for the Tl 4f core level shows two symmetrical peaks corresponding to Tl $4f_{7/2}$ and Tl $4f_{5/2}$ with a spin−orbit splitting of ≈4.4 eV. The measured binding energies for the Tl $4f_{7/2}$ core level after correcting for the C 1s (284.6 eV) peak are 117.6 and 117.5 eV for films grown at 0.05 and 5 mA/cm^2, respectively. The measured binding energies are consistent with the reported value of 117.4 eV for the oxidation state of +3 for Tl in the literature.[24,25] Similarly, the energy spectrum for the Pb 4f core level shows two symmetrical peaks corresponding to Pb $4f_{7/2}$ and Pb $4f_{5/2}$ with a spin−orbit splitting of ≈4.9 eV. The measured binding energies for the Pb $4f_{7/2}$ core level after correcting for the C 1s (284.6 eV) peak are 137.2 and 137.1 eV for the films grown at 0.05 and 5 mA/cm^2, respectively. The measured binding energies are consistent with the reported value of 137.1 ± 0.3 eV for the oxidation state of +4 for Pb in the literature.[24,26] The O 1s peak position observed at 528.5 eV agrees well with the literature values of 528.5 ± 0.3 eV for PbO_2.[26] A small fwhm of ≈1.2 eV for the elements is suggestive of a uniform chemical environment for various atoms on the surface of the film.

Quantitative analysis for evaluating the film compositions on a metals-only basis from XPS were based on

(24) Moulder, J. F.; Stickle, W. F.; Sobol, P. E.; Bomben, K. D. *Handbook of X-ray Photoelectron Spectroscopy*; Chastain, J., Ed.; Perkin-Elmer Corporation: Eden Prairie, MN, 1992.
(25) Young, K. H.; Smith, E. J.; Eddy, M. M.; James, T. W. *Appl. Surf. Sci.* **1991**, *52*, 85.
(26) Malitesta, C.; Sabbatini, L.; Zambonin, P. G. *J. Chem. Soc., Faraday Trans.* **1989**, *85*, 1685.

the measured areas for the Pb $4f_{7/2}$ and Tl $4f_{7/2}$ peaks. The determination of the relative amount of oxygen is subject to large errors as inclusion of oxygen would require a much larger quantification region (≈450 eV). Also, the low intensity of the O 1s peak value makes the quantitative determination of oxygen unreliable. The measured areas for the Pb and Tl were corrected for the reduced sensitivity factor (RSF) before normalizing to obtain the percentage atomic composition for the films. The RSF values used were 5.19 for Pb $4f_{7/2}$ and 4.80 for Tl $4f_{7/2}$. Shirley background correction was performed to measure the peak area. The compositions for the films grown at 0.05 and 5 mA/cm^2 are $Pb_{0.45}Tl_{0.55}O_{1.7}$ and $Pb_{0.8}Tl_{0.2}O_{1.9}$, respectively. The compositions by XPS for the films grown at different current densities are in good agreement with the values listed in Table 1 for the film compositions determined using EDS and ASV.

Superlattices in the Pb−Tl−O system were electrodeposited on Au(100) by periodically pulsing the current density between 0.05 and 5 mA/cm^2. The first layer was intentionally grown at a lower driving force to obtain a smooth and uniform initial layer. The initial layer grown at 0.05 mA/cm^2 for t_a seconds has thickness λ_a and a lower Pb/Tl ratio. The second layer grown at 5 mA/cm^2 for t_b seconds has thickness λ_b and a higher Pb/Tl ratio. The modulation wavelength Λ_F for the superlattice is the sum of individual layers. For the electrochemically deposited films the modulation wavelength can be calculated using eq 1, which is derived from Faraday's law,

$$\Lambda_F = \lambda_a + \lambda_b = 1/nF(j_a M_a t_a/\rho_a + j_b M_b t_b/\rho_b) \quad (1)$$

where n is the number of electrons transferred, F is Faraday's number, j is the applied current density, M is the formula weight, and ρ is the density. For the superlattices reported in the current work, dwell times at different current densities have been adjusted to give approximately the same thickness for individual layers.

The artificially imposed periodicity in the system gives rise to satellite peaks that are symmetric around the Bragg reflection. These satellite peaks show the crystallographic coherence of the deposited multilayers and confirm the superlattice structure of the electrodeposited film.[27−29] The modulation wavelength for the deposited films can be calculated from the positions of these satellite peaks using eq 2,

$$\Lambda_x = \lambda(N_+ - N_-)/(\sin\theta_+ - \sin\theta_-) \quad (2)$$

where N_+ and N_- are the satellite orders, λ is the wavelength of the incident X-rays, and θ_+ and θ_- are the positions of the high-angle (+) and low-angle (−) satellites on the 2θ scan. Figure 2A shows the X-ray 2θ scan for a film grown by pulsing the current between 0.05 (150 s) and 5 mA/cm^2 (1.5 s). The film has a strong [100] out-of-plane orientation. Figure 2B shows the scan on a logarithmic scale for the same film around the (400) reflection of Pb−Tl−O. The modulation wavelength

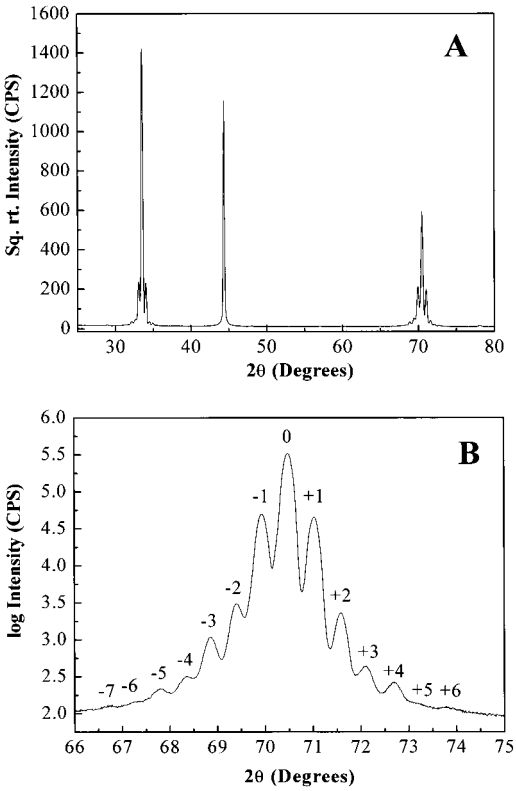

Figure 2. (A) X-ray 2θ scan for Pb−Tl−O superlattice deposited by pulsing the current between 0.05 (150 s) and 5 mA/cm^2 (1.5 s). (B) 2θ scan around the (400) reflection for Pb−Tl−O showing seven orders of satellite peaks. The modulation wavelength, Λ_x, (i.e., the bilayer thickness) calculated from the satellite spacing is 18.9 nm.

calculated from the first-order satellite peaks is 18.9 nm. Seven orders of satellite peaks are clearly seen, with the intensity of the first satellite peak ≈13% of the intensity of the Bragg reflection. The observation of satellites in X-ray diffraction suggests that the electron density is modulated in the superlattices. Because Tl(III) and Pb(IV) are isoelectronic, the main cause of X-ray contrast in this system may be the variation of the oxygen content in the alternating layers. If Tl and Pb are viewed collectively as M, the composition of the films can be represented as $MO_{1.7}$ and $MO_{1.9}$ for the layers deposited at 0.05 and 5 mA/cm^2, respectively. A material with an ideal fluorite structure would have a composition of $MO_{2.0}$.

The fwhm of the Bragg peak is a measure of the structural coherence in the growth direction. The fwhm for the (400) reflection of Pb−Tl−O in Figure 2 is 0.2224°. The irregularity in the thicknesses of the different layers results in out-of-phase diffraction of the incident X-rays. The coherence length gives the measure of layers that diffract X-rays beam coherently (i.e., in-phase) and determines the width of the Bragg peak in the 2θ scan.[5] The radial width of the zeroth-order peak was used to calculate the coherence length, L, using eq 3,

$$L = 2\pi/\Delta q \quad (3)$$

where q is the scattering vector given by $q = 2\pi/d$, d is the lattice parameter in Å, and Δq is the peak width in the radial scan.[30] The effect of instrumental broadening[5]

(27) Lashmore, D. S.; Dariel, M. P. *J. Electroc. Soc.* **1988**, *135*, 1218.
(28) Segmuller, A.; Krishna, P.; Esaki, L. *J. Appl. Crystallogr.* **1977**, *10*, 1.
(29) Schuller, I. K.; Falco, C. M. *Surf. Sci.* **1982**, *113*, 443.

Table 3. Deposition Parameters for Different Modulation Wavelengths and the Comparison of the Modulation Wavelength by Faraday's Law (Λ_F) and X-ray Diffraction (Λ_x)

dwell time at 0.05 mA/cm^2 (s)	dwell time at 5 mA/cm^2 (s)	Λ_F (Faraday's law) (nm)	Λ_x (X-ray data) (nm)	coherence length (L) (nm)
150	1.5	17.8	18.9	28
75	0.75	8.9	9.6	18
40	0.5	5.3	5.2	22

on the peak width at high angle was accounted by using eq 4 for a Gaussian peak profile,

$$\Delta q^2 = \Delta q_{obs}{}^2 - \Delta q_{ins}{}^2 \quad (4)$$

where Δq_{obs} is the measured fwhm in the radial scan and Δq_{ins} is the fwhm for a standard specimen such as a Si or Ge single crystal. The value of Δq_{ins} is measured at a q value comparable to the one used for the specimen. A value of $\Delta q_{ins} = 0.00209$ (Å^{-1}) was determined from the (400) reflection, $2\theta = 69.132°$, of single-crystal Si(100). The coherence lengths for the three superlattices of varying modulation wavelengths are shown in Table 3. The coherence lengths for the first two films are approximately twice the modulation wavelength Λ_x, while the coherence length for the third film with $\Lambda_x = 5.2$ nm is ≈5 times the modulation wavelength Λ_x. The results are consistent with the trend obtained for metallic superlattices grown by MBE[30] where the ratio of coherence length to modulation wavelength decreases with increasing modulation wavelength.

The quality of the out-of-plane orientation can be probed using rocking scans. The mosaic spread and the lateral size of the coherently diffracting layers determine the fwhm of the peak in the rocking scans.[5,30] Figure 3A,B shows the rocking scans for the (200) reflections of Au(100) and Pb−Tl−O ($\Lambda_x = 18.9$ nm), respectively. The fwhm for the (200) reflection of Au(100) single crystal was determined by setting $2\theta = 44.392°$ and rocking the sample along the ω axis. The fwhm for the Au(200) reflection is 0.5530°. The same procedure for the (200) reflection of the Pb−Tl−O superlattice gives a fwhm of 0.9224°. The other important thing to note is the absence of superlattice peaks in the rocking scan for the Pb−Tl−O superlattice. For a nearly perfect superlattice structure satellite peaks should be observed in the rocking curves.[31] The classic example of such a system is a AlGaAs/GaAs superlattice grown on single-crystal GaAs by molecular beam epitaxy. The absence of these peaks could be attributed to the large mosaic spread for the Pb−Tl−O superlattice.

The in-plane orientation of the electrodeposited superlattices can be probed by running an X-ray pole figure. Pole figures are run by choosing a diffraction angle, 2θ, corresponding to the d spacing of the plane of interest. The tilt of the sample, χ, is then incrementally varied, with the azimuthal angle, ϕ, varied from 0 to 360° at each value of χ. Peaks occur in the pole figure when the Bragg condition is satisfied. Figure 4A is the

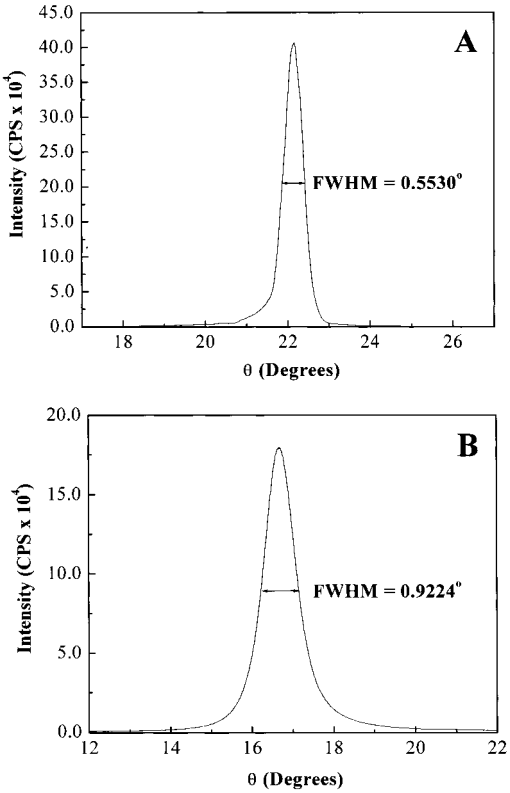

Figure 3. (A) X-ray rocking scan for the (200) reflection of Au(100) at $2\theta = 44.392°$. The mosaic spread for the Au substrate is 0.5530°. (B) Rocking scan for the (200) reflection of the Pb−Tl−O superlattice with $\Lambda_x = 18.9$ nm at $2\theta = 33.5636°$. The mosaic spread of the superlattice is 0.9224°.

(111) pole figure for the superlattice with a modulation wavelength of 18.9 nm. The diffractometer was set at a fixed $2\theta = 28.9306°$ corresponding to the (111) peak position for Pb−Tl−O. The sample was then rotated azimuthally from 0 to 360° at a step size of 1°/s at each value of χ. The tilt angle, χ, was varied from 0 to 85° at a step size of 1°. In a cubic structure the angle between the (111) and (100) planes is 54.7°. The (111) pole figure presented in Figure 4A shows four peaks each separated 90° azimuthally ($\Delta\phi \approx 90°$) at $\chi \approx 55°$. This is consistent with the 4-fold symmetry expected for the [100] orientation and provides direct evidence of the in-plane orientation of the superlattice. The (111) pole figure for a [100] oriented film with a fiber texture would show a ring of intensity at $\chi \approx 55°$.

Azimuthal scans for the (111) reflections of Au and Pb−Tl−O gives the epitaxial relationship between the film and substrate. Figure 4B shows superimposed azimuthal scans acquired for the (111) reflections of Au and Pb−Tl−O. The azimuthal scan for Au was run by setting the diffractometer at $2\theta = 38.184°$, corresponding to the (111) peak position for Au. The sample was then rotated azimuthally from 0 to 360° at a step size of 1°/s at tilt angle $\chi = 55°$. A similar scan for the (111) reflection of Pb−Tl−O was acquired at $2\theta = 28.9306°$ and tilt angle $\chi = 55°$. The expected 4-fold symmetry is observed for the substrate and the film at $\chi \approx 55°$. The reflections for Pb−Tl−O peaks are rotated 45° azimuthally with respect to Au reflections. The peak-to-background ratio of the measured intensities ($I_{peak}/I_{background}$) in the azimuthal scan is a good indicator of the nature of the epitaxy. A material with a fiber texture

(30) Lamelas, F. J.; He, H. D.; Clarke, R. *Phys. Rev. B* **1991**, *43*, 12296.
(31) Tanner, B. K.; Bowen, D. K. *High-Resolution X-ray Diffractometry and Topography*; Taylor & Francis: London, 1998.

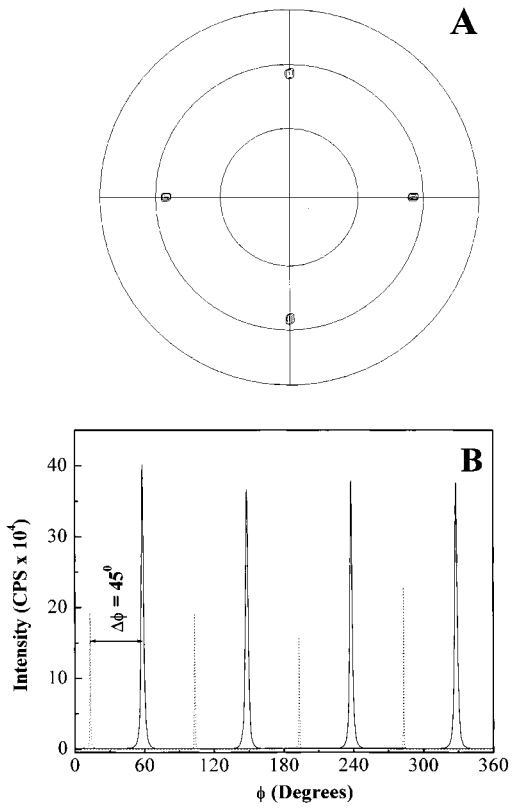

Figure 4. (A) X-ray pole figure on a linear scale for the (111) reflection of Pb−Tl−O superlattice with modulation wavelength (Λ_x) of 18.9 nm. The presence of four symmetric peaks at an approximate tilt angle, χ, of 55° confirm the [100] in-plane orientation for the Pb−Tl−O superlattice. The radial grids on the pole figures represent 30° increments in the tilt angle, χ. (B) Azimuthal scans on a linear scale for the (111) reflections for Au, shown in the dotted line and Pb−Tl−O the solid line. A 45° rotation for the film relative to the substrate is evident in the scans.

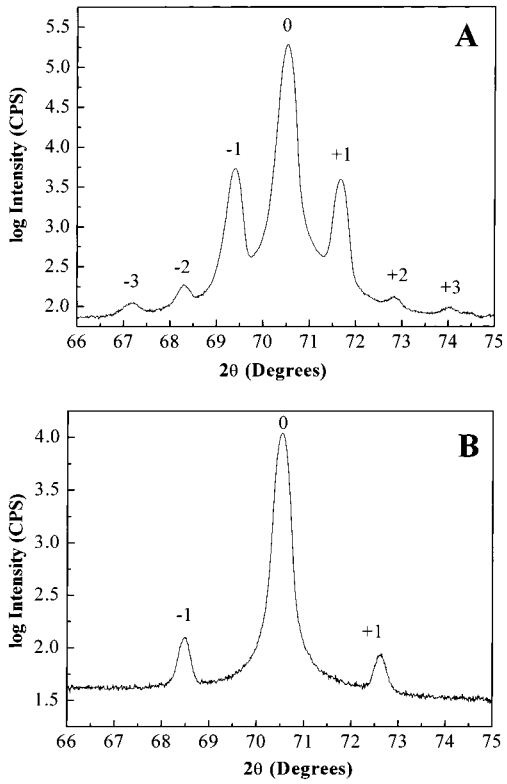

Figure 5. X-ray 2θ scans for Pb−Tl−O superlattices with different modulation wavelengths. (A) The deposition current was pulsed between 0.05 mA/cm^2 (75 s) and 5 mA/cm^2 (0.75 s), $\Lambda_x = 9.6$ nm. (B) The deposition current was pulsed between 0.05 (40 s) and 5 mA/cm^2 (0.5 s), $\Lambda_x = 5.2$ nm.

has a $I_{peak}/I_{background}$ of unity. Consistent with the strong in-plane orientation is the high $I_{peak}/I_{background} \approx 1100$ for the Pb−Tl−O reflection. The similarities in the background intensities for the Au and Pb−Tl−O reflections is an indication of very little or no fiber texture in the electrodeposited superlattice. The fwhm on the azimuthal scans for the Pb−Tl−O and the Au peaks are 2.5° and 0.7°, respectively. The azimuthal scan shows that although the film adopts the same out-of-plane orientation as the substrate, it is rotated 45° in-plane relative to the substrate. An epitaxial relationship consistent with this rotation is Pb−Tl−O(100)[011]//Au-(100)[010]. The in-plane rotation of 45° gives a mismatch of −7.6% compared to the 31% mismatch with no in-plane rotation with respect to Au. Similar results on Au-(100) have been obtained for epitaxially electrodeposited Tl_2O_3 and α-PbO_2.[32,33]

The superlattice modulation wavelength was varied by changing the dwell times at the two deposition current densities. Figure 5A,B shows the satellite peaks for the (400) reflection of the Pb−Tl−O superlattice having modulation wavelengths (Λ_x) of 9.6 and 5.2 nm, respectively. First-order satellite peak positions were used to calculate the modulation wavelength. The films show a strong [100] out-of-plane orientation. The coherence length in the growth direction is listed in Table 3. Also shown in Table 3 is the comparison of the Faradaic and X-ray modulation wavelengths. Modulation wavelengths using Faraday's law were based on the film compositions measured by EDS (Table 1). The small difference in the modulation wavelength on Au(100) calculated from Faraday's law and X-ray diffraction in the present work can be attributed to the lack of precise control over the electrochemically active area while positioning the electrode using the meniscus method. Modulation wavelengths of the Pb−Tl−O superlattices on stainless steel have been previously measured by X-ray diffraction and scanning tunneling microscopy.[19] The measured modulation wavelengths agreed well with the value determined from Faraday's law, giving a 100% current efficiency.

We have shown that it is possible to electrodeposit epitaxial superlattices in the Pb−Tl−O system onto single-crystal Au(100) by periodically pulsing the current density in a single plating bath. Thallium-rich layers were deposited at low current densities and lead-rich layers were deposited at high current densities. The mismatch between the alternating layers was only 0.12%. XPS results are consistent with oxidation states of +4 for Pb and +3 for Tl. Film compositions at different current densities obtained from XPS are in close agreement with those reported from energy-dispersive spectroscopy (EDS) and anodic stripping voltammetry (ASV). The modulation wavelengths were varied from 5.2 to 18.9 nm by controlling the dwell times

(32) Vertegel, A. A.; Bohannan, E. W.; Shumsky, M. G.; Switzer, J. A. *Electrochim. Acta* **2000**, *45*, 3233.
(33) Vertegel, A. A.; Bohannan, E. W.; Shumsky, M. G.; Switzer, J. A. *J. Electrochem. Soc.* **2001**, *148*, 253.

at the respective current densities. The same procedure should be applicable to the epitaxial electrodeposition of magnetic superlattices based on half-metallic ferrimagnetic materials such as Fe_3O_4[34,35] for spintronic applications.

Acknowledgment. This work was supported by NSF grants CHE-9816484, DMR-0071365, and DMR-0076338 and the Foundation for Chemical Research.

CM020042H

(34) Nikiforov, M. P.; Vertegel, A. A.; Shumsky, M. G.; Switzer, J. A. *Adv. Mater.* **2000**, *12*, 1351.

(35) Sorenson, T. A.; Morton, S. A.; Waddill, G. D.; Switzer, J. A. *J. Am. Chem. Soc.*, in press.